Journal of Geomine (2024), 2(3), 176-190
DOI: 10.22077/jgm.2025.9499.1049

Numerical analysis of time-dependent behavior of salt cavern with weak interlayer

Afsaneh Fakhimi[1], Morteza Ahmadi[2], Ehsan Taheri[2]

Recived: 2025 May 28, Revised: 2025 Jul. 15, Online Published: 2025 Jul. 15

ABSTRACT

Natural gas consumption fluctuates due to seasonal demand, extraction limitations, price changes, and political conflicts. These fluctuations necessitate the storage of natural gas. Among various storage methods, salt caverns have several advantages for storing hydrocarbons compared to other methods. These advantages include the low permeability of rock salt and the low cost of construction. However, salt caverns may be affected by weak layers such as marl or mudstone within the formation's layering sequence. This research aimed to numerically study the long-term behavior of a salt cavern excavated in interbedded salt rock with weak interlayers. The effects of placement angle (0°, 30°, 45° and 60°), layer thickness (10, 15 and 20 meters), number of (1 or 2 or 3) and three different levels on operational time were analyzed. FLAC3D finite difference software was selected because of its Cpower creep behavior model. A total of twenty-two numerical models were executed. The results emphasize the importance of level, placement angle, thickness and interlayers numbers on displacement, stability and safety of a salt cavern over its operational time. The Ratigan dilatancy safety factor is not suitable for assessing the effects of geometric parameters of interlayers on salt cavern stability. Generally, constructing a cavern in salt layers containing weak interlayers is not recommended.

KEYWORDS

Gas storage, salt layer, weak interlayer, numerical modeling and creep

I. INTRODUCTION

Natural gas, as a critical energy carrier plays a fundamental role in supplying energy to countries. The imbalance between natural gas supply and demand, strategic storage requirements, extraction restrictions from gas fields, and market fluctuations make underground storage a suitable solution for managing surplus energy (Plaat, 2009).

Gas storage in salt caverns has become an important and widely studied subject because this method provides an ideal storage space by creating an isolated environment with minimal interaction with the surrounding ecosystem. It can be used for strategic storage as well as for adjusting gas supply during peak consumption periods. Rock salt deposits are influenced by geological factors and exist in various forms. Depending on sediment thickness, they can be categorized as either salt domes or interbedded salt formations (Wei et al., 2016). When rock salt and interlayers (such as mudstone) experience stress, they deform differently. Over time, these deformations can impact the stability and safety of storage caverns (Xing et al., 2015).

Langer and Heusermann (2001) investigated the stability of salt caverns. They emphasized that the mechanical parameters of rock salt and the stresses affecting cavern stability are crucial factors (Langer & Heusermann, 2001).

Wang et al. (2011) investigated how rock salt deforms in the presence of interlayers, specifically around gas and oil storage caverns. They found that the development of plastic zones and dilatation in rock salt is influenced by the geomechanical properties of the interlayer. Additionally, the stiffness of the overburden rock mass significantly affects stress arching on the cavern roof, as well as cavern convergence and surface subsidence over time (Wang et al., 2011). Ma et al. (2012) studied the convergence of underground gas storage caverns in deep-layered rock salt formations, aiming to understand volume convergence behavior at high temperatures and pressures. High-temperature creep tests and numerical simulations were conducted to analyze the effects of temperature and deviatoric stress on cavern convergence of salt caverns. The results showed that increasing either deviatoric stress or the temperature leads to a higher steady-state creep rate, with deviatoric stress having a greater influence. The volume convergence process follows a pattern similar to creep curves, which initially increase rapidly and then slow over time (Ma et al., 2012).

[1] MSc. Rock Mechanics, Mining Eng., Mining and Materials Eng. Faculty, Tarbiat Modares, Tehran, Iran, [2] Rock Mechanics Gr., Mining Eng., Mining and Materials Eng. Faculty, Tarbiat Modares, Tehran, Iran

✉ A. Fakhimi: Afsaneh.fakhimi@modares.ac.ir

Li et al. (2015) emphasized the importance of predicting and controlling ground subsidence above storage caverns to ensure long-term performance. They modeled the salt cavern as either spherical or cylindrical to simplify analytical solutions for calculating ground subsidence and studied the effects of internal gas pressure (Li et al., 2015).

Zhang et al. (2015) examined the effects of impurities and rock salt creep, as well as ground subsidence above gas storage salt caverns and the effects of various factors on this subsidence. They assumed a spherical cavern and developed a relationship to calculate volume reduction during construction and operation (Zhang et al., 2015).

Shahmorad et al. (2016) investigated the stability of a salt gas cavern, focusing on the effects of Berger's behavioral model and the WIPP empirical model. They found that the power model provides a more conservative stability analysis (Shahmorad et al., 2016).

Liang et al. (2016) developed a 3D geomechanical model using FLAC3D software to evaluate the long-term stability of a natural gas storage cavern in interbedded salt rock. Their research focused on deformations caused by rock salt creep and stability evaluation criteria, including displacement, convergence rate, safety factor, and safe column width between caverns. The results indicated that cavern construction should be avoided in areas with a high density of mudstone interlayers. However, if the mudstone interlayer has high strength and reduces cavern convergence, the cavern may be feasible (Liang et al., 2016).

Yang et al. (2016) conducted a stability analysis on a group of closely spaced caverns using numerical modeling. They modeled four salt caverns in ANSYS, spacing them at 0.7 times their maximum diameter. The model included two mudstone interlayers at the top and bottom of each cavern. They used a three-dimensional geomechanical numerical model to simulate and validate the design, considering factors such as deformations, volume reductions, and safety under various conditions. The findings suggested that this design could double the number of caverns compared to conventional designs, thus substantially increasing storage capacity(Yang et al., 2016).

Mortazavi et al 2017 examine the design and stability of underground oil storage caverns constructed in salt rock, highlighting their safety due to salt's low permeability and strong mechanical properties. The research uses 3D numerical modeling to explore how factors like cavern size, depth, and stress conditions affect stability. The safety factor of caverns decreases as the depth and size of the caverns increase. Stability improves when the horizontal-to-vertical stress ratio is lower. The sensitivity to stress ratios reduces as the Young's modulus of the salt rock becomes higher (Mortazavi & Nasab, 2017).

Salt rocks in China are primarily found in layer formation. Zhang et al. (2017) researched the stability and construction of salt caverns within these formations, identifying them as suitable environments for creating oil storage caverns (Zhang et al., 2017).

Wang et al. (2018) analyzed the safety factor of gas storage salt caverns in deep stratified salt formations. These factors included displacement, cavern convergence, plastic zone, and equivalent strain. Their findings revealed that the dilation factor decreases as the diameter of the cavern increases, leading to maximized areas of high displacement. The presence of interlayers with high strength and enough thickness in the upper part of the cavern helps to control displacements. Additionally, a greater stress concentration is observed at the interface between the interlayer and rock salt (Wang et al., 2018).

Liu et al. (2020) investigated the feasibility of using irregular-shape caverns for gas storage. They examined four underground caverns with different shapes, which were constructed by dissolution in salt formations and have irregular shapes due to complex geographical conditions. The results showed that the shape of the cavern significantly affects its stability. Various methods, including optimizing the cavern shape, reinforcement of the surrounding rock and controlling the internal pressure of the cavern, were used to increase stability (Liu et al., 2020).

Li et al. (2021) used a geomechanical model to investigate the stability of a horizontal natural gas storage cavern. They used 3D modeling using FLAC3D software and the Cpower behavioral model. This research focused on the effects of cyclic and constant pressure changes on stability indicators such as displacement, Dilatancy safety factor, volume contraction, plasticity area, and equivalent strain. The results indicated that the frequency of the loading-unloading cycle significantly affects the stability of the horizontal cavern. Although the cavern location was in interbedded salt rock, the effects of the interlayer on the stability and shape of the cavern were not considered in this study (P. Li et al., 2021).

Zhou et al. (2022) analyzed the stability of a salt cavern in an interbedded salt rock environment. This research investigated the deformation rate of the cavern under various interlayer conditions, including thickness, placement angle, number and strength of interlayers. The results showed that the presence of interlayers causes stress concentration. Therefore, it is advised to avoid to construct salt caverns in a media with numerous or thick interlayers (Zhou et al., 2022).

Peng et al. (2023) investigated the effect of interlayers on the long-term stability of salt caverns. They studied the effects of interlayer thickness, placement angle, stiffness, the distance between two caverns, and the pressure difference between caverns. The results indicated that an interlayer with lower

stiffness increases cavern deformation, whereas an interlayer with higher stiffness increases the deformation rate (Peng et al., 2023).

While many researchers have studied the mechanical properties of rock salt and utilized numerical analysis to examine the stability of salt caverns, research on the effect of interlayers on their long-term stability has been limited. This study aims to study how the mechanical characteristics and geometric configurations of interlayer such as thickness, placement angle, level and number of layers influence the displacement and stability of salt cavern.

II. Numerical Analysis

The FLAC3D finite difference software is highly effective at accurately simulating the time-dependent deformation of rocks. It includes eight behavioral models for creep simulation, namely:

- Two-component power model
- Viscous model
- Burger model
- WIPP model
- PWIPP model
- Visco-plastic power model (Cpower)
- Visco-plastic Burger model (Cvisc)
- CWIPP model

A. Constitutive Model

A constitutive model describes how a material responds to stress. The creep behavior model focuses on the deformation over time. The visco-plastic power model combines the elastoplastic response from the Mohr-Coulomb model with the visco-elastic behavior of the two-component power model. This model is helpful because it has limited parameters and does not include complex temperature variables. The total strain rate has three components (Zhou et al., 2022): elastic $\dot{\varepsilon}^{e}{}_{ij}$, viscous $\dot{\varepsilon}^{c}{}_{ij}$, and plastic $\dot{\varepsilon}^{p}{}_{ij}$.

$$\dot{\varepsilon}_{ij} = \dot{\varepsilon}^{e}{}_{ij} + \dot{\varepsilon}^{c}{}_{ij} + \dot{\varepsilon}^{p}{}_{ij} \quad (1)$$

Only the elastic component contributes to the strain rate, while the deviatoric stress causes visco-elasto-plastic behavior.

$$q = \sqrt{3J_2} \quad (2)$$

$$\dot{s}_{ij} = 2G(\dot{e}_{ij} - \dot{e}^{c}{}_{ij} - \dot{e}^{p}{}_{ij}) \quad (3)$$

$$\dot{e}^{C}_{ij} = \dot{e}_{cr}\frac{\partial q}{\partial s_{ij}} \quad (4)$$

$$\frac{\partial q}{\partial s_{ij}} = \frac{3}{2}\frac{s_{ij}}{q} \quad (5)$$

The terms $\dot{s}_{ij}$ and $\dot{e}_{ij}$ denote the deviatoric components of the stress and strain rate ($\dot{\sigma}_{ij}$ and $\dot{\varepsilon}_{ij}$) respectively. The symbol G represents the shear modulus. The relationship between the Von Mises stress (q) and the reference stress levels influences the activation of creep behavior. When the von Mises stress exceeds the reference stress levels, the material begins to deform plastically, and creep behavior is activated. σ_1^{ref}, σ_2^{ref} represent reference stress levels. J_2 is second invariant of stress deviatoric tensor.

The creep intensity of the Cpower model is written as:

$$\dot{e}_{cr} = \dot{e}^{1}_{cr} + \dot{e}^{2}_{cr} \quad (6)$$

$$\dot{e}^{1}_{cr} = \begin{cases} A_1 q^{n_1} & q \geq \sigma_1^{ref} \\ 0 & q < \sigma_1^{ref} \end{cases} \quad (7)$$

$$\dot{e}^{2}_{cr} = \begin{cases} A_2 q^{n_2} & q \leq \sigma_2^{ref} \\ 0 & q > \sigma_2^{ref} \end{cases} \quad (8)$$

A_1, A_2, n_1 and n_2 are rheological parameters. The stress exponents n_1 and n_2 are important for describing how the creep rate varies with applied stress. The exponent n_1 and parameter A_1 are associated with the primary creep stage, during which the creep rate decreases over time. In contrast, the exponent n_2 and parameter A_2 correspond to the secondary (steady-state) creep stage.

The Mohr-Coulomb flow law defines the plastic strain rate:

$$\dot{e}^{p}_{ij} = \dot{e}_P\frac{\partial g}{\partial \sigma_{ij}} - \frac{1}{3}\dot{e}^{p}_{vol}\delta_{ij} \quad (9)$$

$$\dot{e}^{p}_{vol} = \dot{e}_P\left[\frac{\partial g}{\partial \sigma_{11}} + \frac{\partial g}{\partial \sigma_{22}} + \frac{\partial g}{\partial \sigma_{33}}\right] \quad (10)$$

The direction of plastic flow $\frac{\partial g}{\partial \sigma_{ij}}$, is expressed using the Mohr-Coulomb potential function (g). The intensity of plastic flow $\dot{e}_P$, is derived from the Mohr-Coulomb yield criterion (Zhang et al., 2021).

III. Stability Analysis

A. Dilatancy Safety Factor

The dilatancy safety factor can be used to evaluate the stability of salt caverns. Dilation (increasing volume) arises from the formation of microcracks and pore expansion under deviatoric stress. This phenomenon can lead to the spalling of cavern roof or walls and potential for gas leakage. Dilatancy poses a threat not only to the safety of the cavern but also to its operational efficiency. Consequently, monitoring and managing dilatancy is fundamental to ensure the stability of caverns. Cyclic loading can affect salt time-dependent behavior, resulting in internal structural changes such as microcrack formation and new pore development, leading to increased volume. The dilatancy safety factor named Ratigan, SF_{vs}, is determined by (I_1), which is the first invariant of stress and is equal to $I_1 = \sigma_1 + \sigma_2 + \sigma_3$. Second invariant of the deviatoric stress (J_2) is defined as follows (P. Li et al., 2021):

$$J_2 = \frac{1}{6}[(\sigma_1 - \sigma_2)^2 + (\sigma_2 - \sigma_3)^2 + (\sigma_3 - \sigma_1)^2] \quad (11)$$

$$SF_{vs} = \frac{0.27I_1}{\sqrt{J_2}} \quad (12)$$

Table 1. presents the threshold dilatancy safety factor alongside the corresponding rock condition(Wang et al., 2016; Yang et al., 2015):

Table 1. Threshold Dilatancy Safety Factor and Corresponding Rock Condition (Wang et al., 2016; Yang et al., 2015).

Level	SF_{vs} Threshold	Rock Condition
1	<0.6	Collapse
2	<1	Failure
3	<1.5	Local Damage

B. Equivalent Strain

Equivalent strain can be used to evaluate the safety of salt cavern and plastic creep behavior. It is beneficial because rock salt, like ductile material, undergoes deformation under in-situ stress. Equivalent strain consolidates various strain components into a single value, providing a comprehensive measure of the overall deformation of the material. The equivalent strain is mathematically expressed as follows (D. Li et al., 2021; Wang et al., 2018):

$$\varepsilon_{eq} = \sqrt{\frac{4}{3}J_2} \quad (13)$$

$$J_2 = 1/6\left[\left(\varepsilon_{xx}-\varepsilon_{yy}\right)^2+\left(\varepsilon_{yy}-\varepsilon_{zz}\right)^2+(\varepsilon_{xx}-\varepsilon_{zz})^2+6\left(\varepsilon_{xy}^2+\varepsilon_{yz}^2+\varepsilon_{xz}^2\right)\right] \quad (14)$$

Where ε_{eq} is equivalent strain and J_2 is the second invariant strain tensor and ε_{xx}, ε_{yy}, ε_{zz}, ε_{xy}, ε_{yz}, ε_{zx} are the components of strain in different directions. The threshold for equivalent strain in salt caverns is generally set at 3% over the operation time. This value is used to ensure the stability and safety of the cavern, preventing excessive deformation and potential failure due to creep (D. Li et al., 2021; Wang et al., 2018).

IV. NUMERICAL MODELING

A capsule-shaped salt cavern with a radius of 30 meters was excavated in a thick salt layer that was 530 meters thick. The cavern center was considered to be located at a depth of 900 meters. An interlayer of mudstone was considered which level (level A, B and C), thickness and placement angle vary in different numerical models. Fig. 1. illustrated the cavern geometry, coordinate axes and level A, B and C.

AutoCAD software was applied to design geometry of model. Subsequently, Rhino and Gridle graphics software were used to mesh the model and convert it into a format compatible with FLAC3D software. Due to the model symmetry and decreasing computational time, only a semi-section of the cavern geometry was constructed. Without defined boundary conditions, the model would undergo significant displacements as it reaches equilibrium due to the stress field. Therefore, it was essential to constrain the model boundaries to prevent movement in the X and Y directions and the floor of the model had to be fixed in all three dimensions.

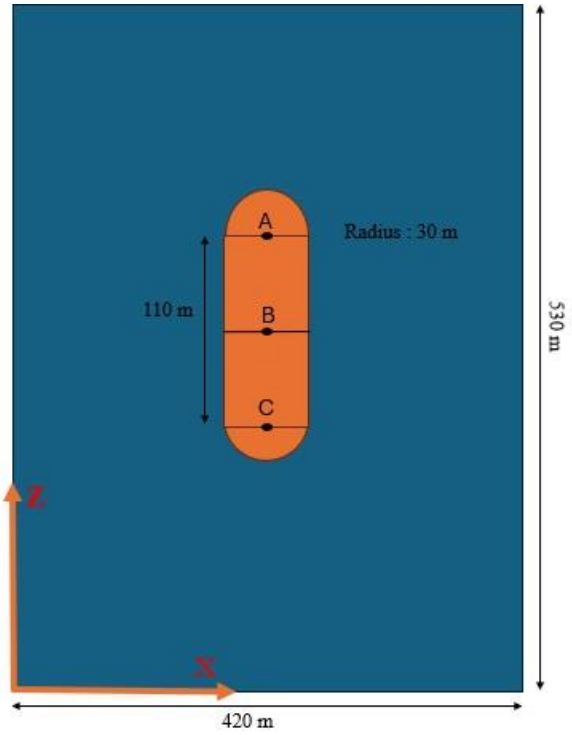

Fig. 1. Schematic of salt cavern model and level A, B and C

Twenty-two numerical model were created to investigate the effects of weak interlayers; thickness, placement angle, level and number of interlayers. Roof of the salt cavern is one of the most critical points due to its vicinity to the casing shoe. The effect of increasing thickness to 10, 15, and 20 meters with placement angles of 0°, 30°, 45° and 60° at level A were investigated. The effect of different placement angles was studied at different levels A, B, and C with a fixed thickness of 10 meters. Additionally, the effect of 1, 2 or 3 interlayers was studied. The Geo0 model without any interlayer was considered as a base model. Table 2. briefly states the geometry conditions of each model.

A. Material Parameters

The typical three-phase creep curve of salt rock includes:

- Initial creep (transient creep)
- Steady-state creep (secondary creep)
- accelerated creep (tertiary Creep)

The steady-state creep stage is the longest phase, with a constant creep rate. This phase is essential for analyzing the long-term behavior of materials, especially salt rock. During this stage, microfractures in the salt rock form and gradually develop until failure occurrs. The main factors affecting stable creep are temperature and deviatoric stress. When the temperature is constant, an increase in deviatoric stress enhances the steady-state creep rate of salt rock. Similarly, if the stress is constant, the creep rate follows a similar pattern. When both factors are constant, the creep rate remains unchanged mainly (Günther et al., 2015; Zhou et al., 2022).

This research focuses on simulating steady-state creep without the effect of temperature, so parameters A_2 and n_2 were used. The gas compressibility or shrinkage effects have been neglected. Based on the data, the interlayer mudstone has a lower elastic modulus compared to rock salt, resulting in greater deformation. The creep order of the mudstone was considered lower than that of rock salt. Consequently, the interlayer will not exhibit brittle or fragile behavior but will gradually creep over time without fracturing.

Table 2. Geometry conditions of models

Model	placement Angle (degrees)	Thickness (m)	Number of interlayers	Level
geo0	-	-	-	-
geo1	0	10	1	A
geo2	0	15	1	A
geo3	0	20	1	A
geo4	30	10	1	A
geo5	30	15	1	A
geo6	30	20	1	A
geo7	45	10	1	A
geo8	45	15	1	A
geo9	45	20	1	A
geo10	60	10	1	A
geo11	60	15	1	A
geo12	60	20	1	A
geo13	0	10	1	B
geo14	30	10	1	B
geo15	45	10	1	B
geo16	60	10	1	B
geo17	0	10	1	C
geo18	30	10	1	C
geo19	45	10	1	C
geo20	60	10	1	C
geo21	0	10	2	B, C
geo22	0	10	3	A, B, C

Table 3. outlines the parameters of the creep behavior model, while Table 4. details the geomechanical properties of rock salt and the weak interlayer (Wang et al., 2018).

Table 3. Parameters of creep behavior model (Wang et al., 2018)

Rock	$A_2(^{MPa}/_{h})$	n_2
Mudstone	2.8×10^{-7}	1.5
Salt rock	5.081×10^{-14}	8.052

In FLAC3D software, static equilibrium denotes a condition where the model has reached a complete static solution. After setting the boundary conditions, in situ stresses were applied to the model. The stress from overburden weight was imposed on the upper boundary of model in *Z* direction, amounting to 16.5 MPa. This was calculated based on 635-meter cavern depth and a density of 2600 kg/m^3. Due to viscous behavior of rock salt at that condition, value of *K* (the ratio of horizontal to vertical stress) was considered equal to 1. The contours of stress and displacement, along with the graph of maximum unbalanced force, were analyzed. As a result, the model successfully converged and reached equilibrium.

B. Pressurizing of Cavern

Determining the minimum pressure is crucial for maintaining convergence of the cavern within acceptable limits and preventing dilatancy. Generally, this minimum pressure should range from 20 to 35% of the overburden pressure at the casing shoe area. The maximum pressure should remain between 75 to 85% of the overburden pressure to avoid the high risk of failure in the salt cavern (Asgari et al., 2020).

Operational time of salt cavern was considered 15 years. During this time, creep deformation of cavern was analyzed. Over time, dissolution extraction has progressed, and the in-situ stresses have gradually decreased until they equilibrated with the stress induced by the brine column. The pressure exerted by the brine column has been determined using the following equation:

$$P = \rho g h \quad (15)$$

Where, ρ=1100 kg/m^3 (density of saline water), g= 10 m/s^2 (gravitational acceleration), h=1165 m (depth from the surface to the cavern bottom).

After substituting the values, the resulting hydrostatic pressure is 12.8 MPa.

During a 14-month construction period, the cavern's internal pressure dropped from the initial in situ stress of 28.2 MPa to 12.8 MPa, corresponding to the brine column pressure. Subsequently, during brine extraction and gas injection, the internal cavern pressure rises to 18 MPa, reaching the maximum operational threshold, which remains steady for two months. Following gas withdrawal, the cavern pressure drops to 8 MPa, maintaining this level for another two months. This cyclic injection-withdrawal process continues for 15 years. Fig. 2. illustrated the variations in the internal pressure of the salt cavern due to successive gas injection and withdrawal cycles. Six points were considered around the cavern for compromising deformation. These points are shown in Fig. 3.

Table 4. Geomechanical parameters of rocks (Wang et al., 2018)

Rock	Elastic Modulus (GPa)	Poisson's Ratio	Cohesion (MPa)	Internal Friction Angle (degrees)	Tensile Strength (MPa)
Mudstone	3.99	0.26	3.67	38.47	1.65
Salt rock	6.37	0.27	2.42	41.30	0.94

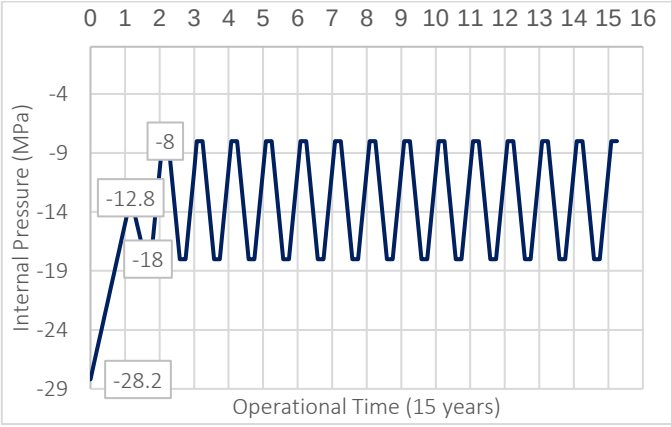

Fig. 2. Gas injection and withdrawal cycles in the salt cavern throughout the operational time

C. *Validation*

To validate the cavern model using recorded data from convergence pins in an actual case was not feasible. Therefore, results of execution model were compared with analytical solution. Using the analytical solution required a simplified model. In this scenario, the salt cavern was modeled as a thick-walled cylinder with an inner radius (a) and an outer radius (b), which had plane strain conditions with stress exerted on its external wall. The following are the equations for the analytical solution (Van Sambeek, 1986):

$$\sigma_r = -P_b + P_b \left[\frac{(b/r)^{2/n} - 1}{(b/a)^{2/n} - 1} \right] \quad (16)$$

$$\sigma_\theta = -P_b - P_b \left[\frac{[(2-n)/n](b/r)^{2/n} + 1}{(b/a)^{2/n} - 1} \right] \quad (17)$$

$$\dot{U}_r = -A(3/4)^{(n+1)/2} \left[P_b \frac{2/n}{(b/a)^{2/n} - 1} \right]^n b^2/r \quad (18)$$

σ_r radial stress, σ_θ tangential stress, $\dot{U}_r$ radial displacement rate, P_b stress is applied to the outer wall, a and b are inner and outer radius, A and n are parameters of the creep model.

The pressure of gas imposed on the internal wall was ($P_a = 28.2$ MPa). The values of (a) and (b) were 30 meters and 210 meters respectively.

Fig. 4. and Fig. 5. illustrated the radial stress and tangential stress versus radius of cylindricalcurve derived from both analytical and numerical methods. The analytical solution confirms that the numerical model is suitable and accurate. Therefore, it can be utilized to design complex conditions such as salt caverns.

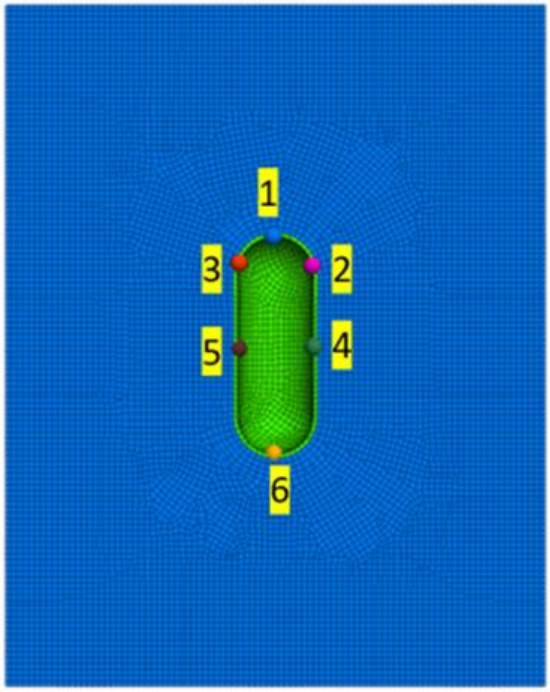

Fig. 3. Location of points around the cavern for compromising deformation

V. RESULTS AND DISCUSSION

A. *Effect of interlayer thickness*

First, the effect of increasing the interlayer thickness (10, 20 and 30 m) at placement angles (0°, 30°, 45° and 60°) was studied. The model of salt cavern without any interlayer (model geo0) had a total deformation of 44 cm. Fig. 6. and Fig. 7. presented the total displacement of salt cavern models geo1 and geo6.

The total deformation of the cavern in the geo1 model increased to 82 cm due to the presence of a horizontal interlayer. Increasing the thickness of the middle layer at a placement angle of 30° increased displacements to 159 cm. Table 5. outlined the displacement changes at level A with variations of thickness and placement angles.

Another key aspect of this investigation is the impact of the interlayer on the displacement components along different spatial directions (e.g., *X*, *Y*, and *Z*). Fig. 8. illustrated how increasing the interlayer thickness affects the wall's displacement along the *X*-axis.

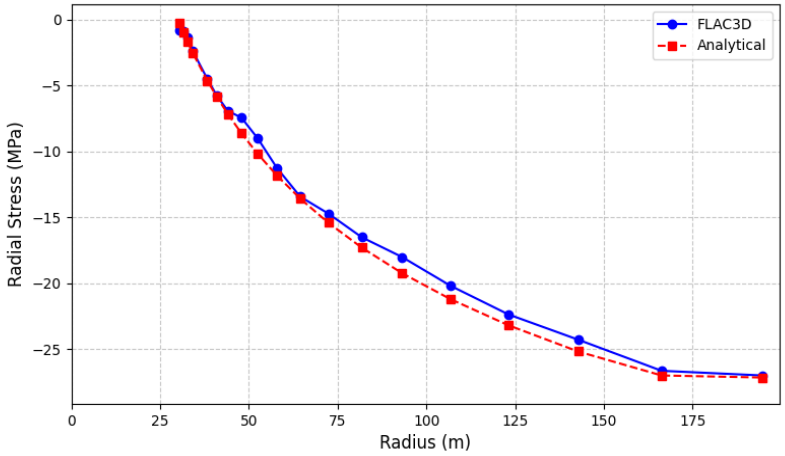

Fig. 4. Comparison of Radial Stress Between Analytical and Numerical Methods

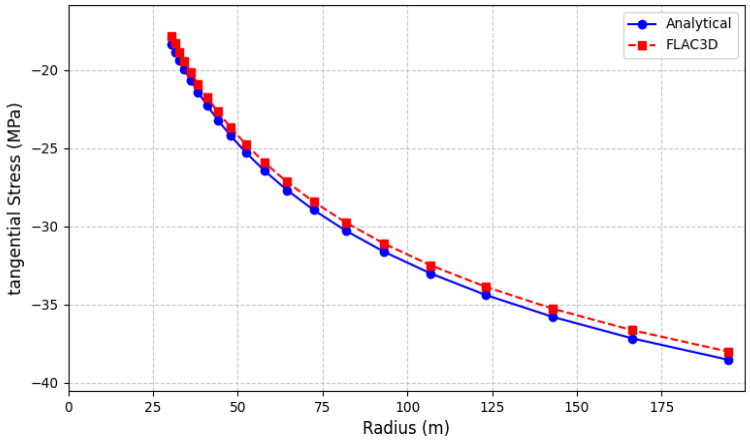

Fig. 5. Comparison of Tangential Stress Between Analytical and Numerical Methods

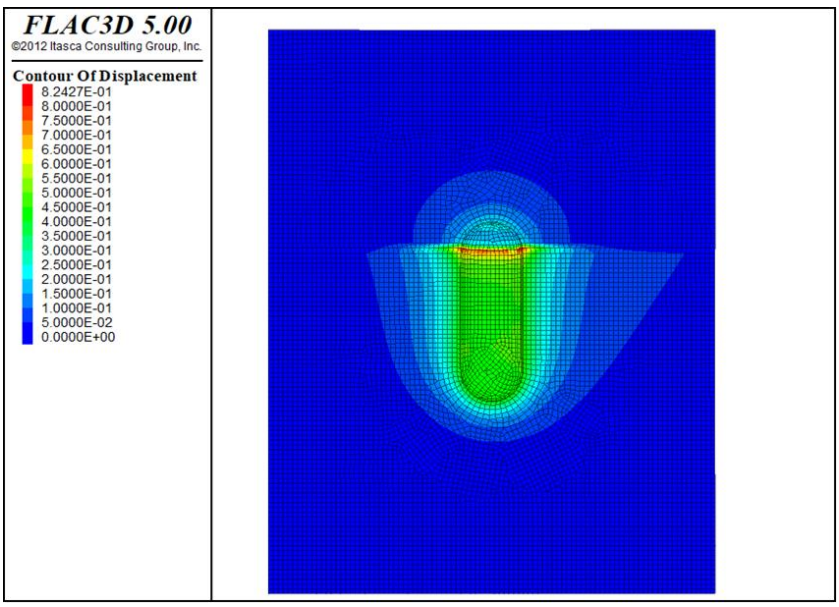

Fig. 6. Total displacement of model geo1 at the end of operational time

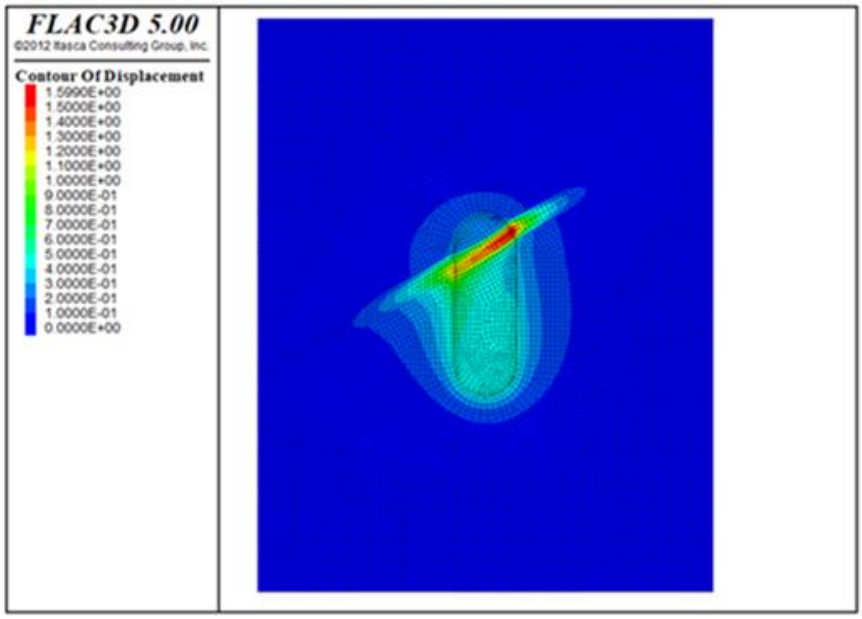

Fig. 7. Total displacement of geo6 model at the end of operational time

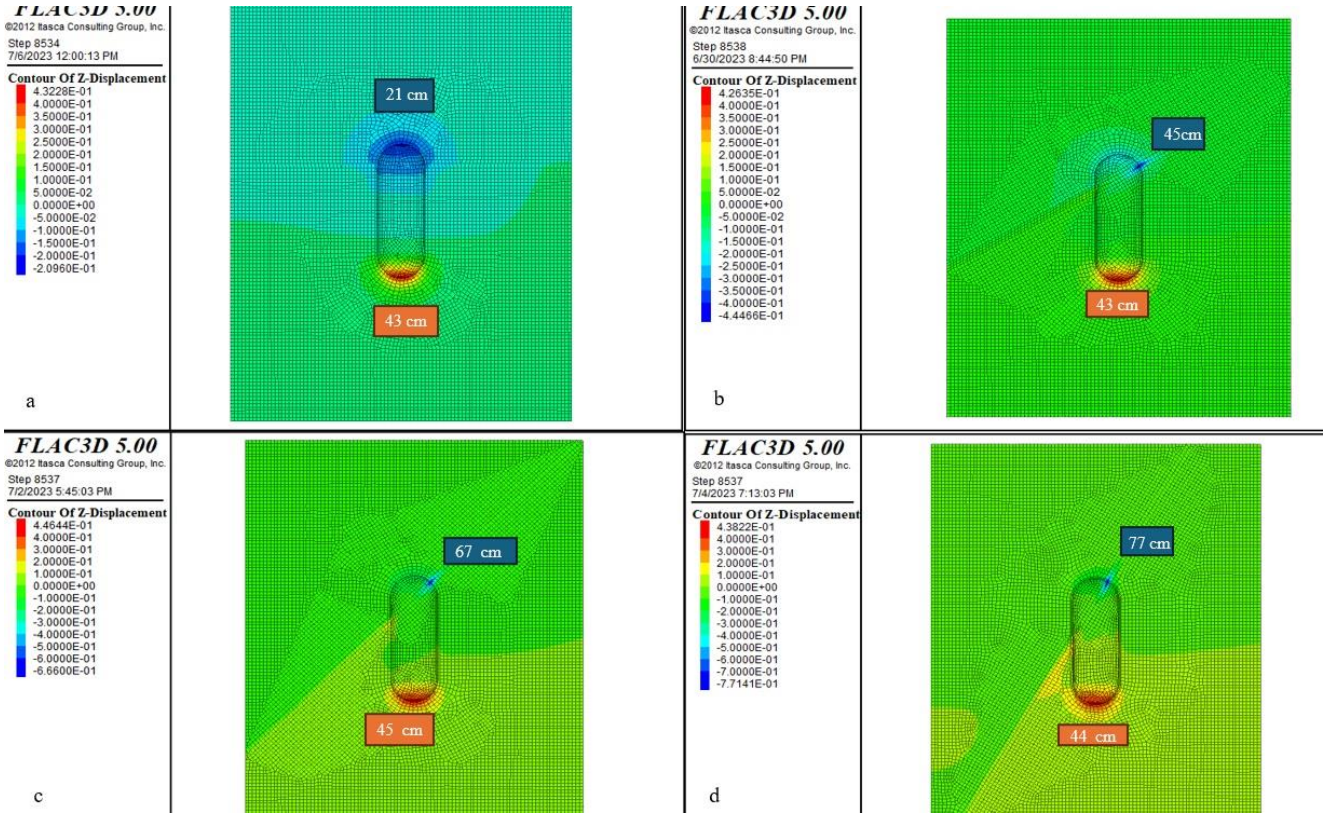

Fig. 8. Effect of increasing interlayer thickness on wall displacement along the X-axis: a) geo0, b) geo1 with an interlayer thickness of 10 meters, c) geo2 with an interlayer thickness of 15 meters, d) geo3 with an interlayer thickness of 20 meters

Table 5. Total displacement (cm) with varying thickness and placement angles at Level A

Thickness (m) / Placement angle (degrees)	10	15	20
0	82	125	150
30	91	130	159
45	94	126	158
60	90	123	155

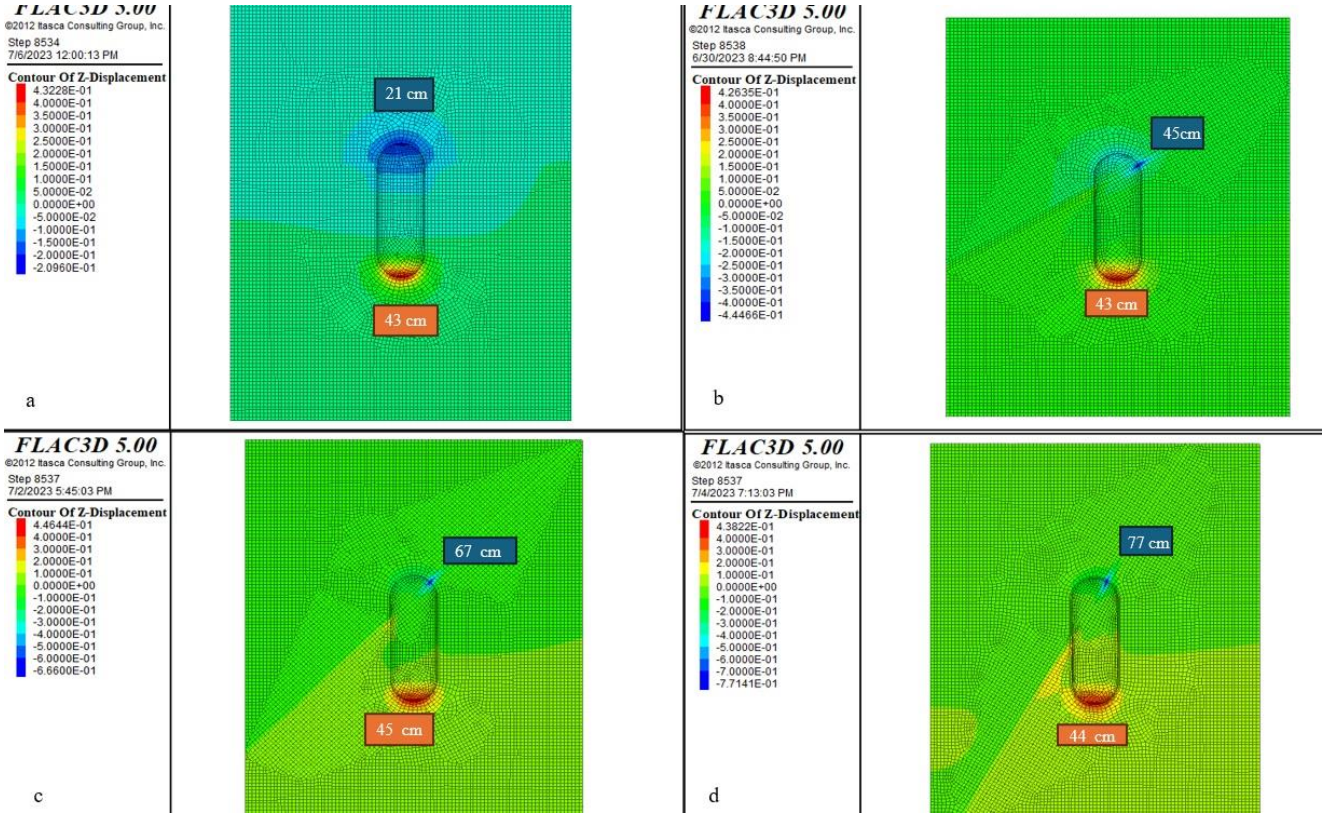

Fig. 9. Effect of different interlayer placement angles on vertical displacement (Z-axis) of the cavern, a) a horizontal interlayer, b) D=30°, c) D=45°, and d) D=60°

Increasing the thickness of the interlayer at level A, located near the roof, leads to greater displacement in all directions (*X*, *Y*, and *Z*) within the vicinity of the interlayer. However, due to its distance from the interlayer's influence radius at level A, the cavern floor remains unaffected by any displacement variations.

B. Effect of different placement angles and different interlayer levels

For studying the effect of different placement angle and different interlayer level, an interlayer of mudstone with 10 m thickness at three levels A, B and C were executed. Fig. 9. illustrated the effect of increasing angle on displacement of cavern wall along *Z*-axis.

At horizontal positioning, displacement values remained relatively low, indicating a stable condition with minimal influence from the interlayer. When the placement angle was 30°, there was a slight increase in displacement, especially in the *X* and *Y* directions. At 45°, the effect became more noticeable, with a significant increase in vertical (*Z*-axis) displacement, suggesting a stronger interaction between interlayer properties and load transfer mechanisms. Finally, at 60°, the steep inclination led to maximum displacement, particularly near the roof of the cavern, demonstrating how increasing the angle directly intensified deformation effects, especially along the *Z* direction. Fig. 10. illustrated the effect of different interlayer level on different directions (*X*, *Y*, *Z*) for models geo10, geo16 and geo20.

Fig. 10. illustrated how the position of the interlayer at different levels (A, B, and C) affected displacement in various directions (*X*, *Y*, and *Z*) at a fixed placement angle of 60°.

- *X*-direction: From Level A to Level C (increasing depth of the interlayer), displacement on the right wall increased. However, the left wall followed a similar trend; its displacement was greater than that of the right wall.
- *Y*-direction: Displacement gradually increased, reaching its maximum value at Level C (119 cm), indicating strong lateral movement.
- *Z*-direction: The roof cavern showed the highest displacement at Level A (77 cm), but this decreased at lower levels. Conversely, the floor cavern followed an opposite trend, with displacement intensifying significantly at Level C (118 cm), demonstrating greater deformation in lower structural regions.

Fig. 11. showed the total displacement at different levels for various placement angles

.

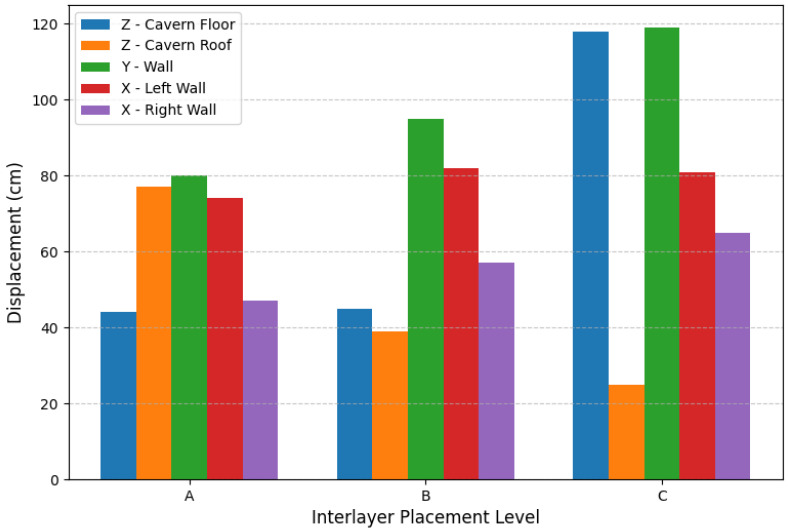

Fig. 10. Effect of different interlayer level at different directions (X, Y and Z) displacemen

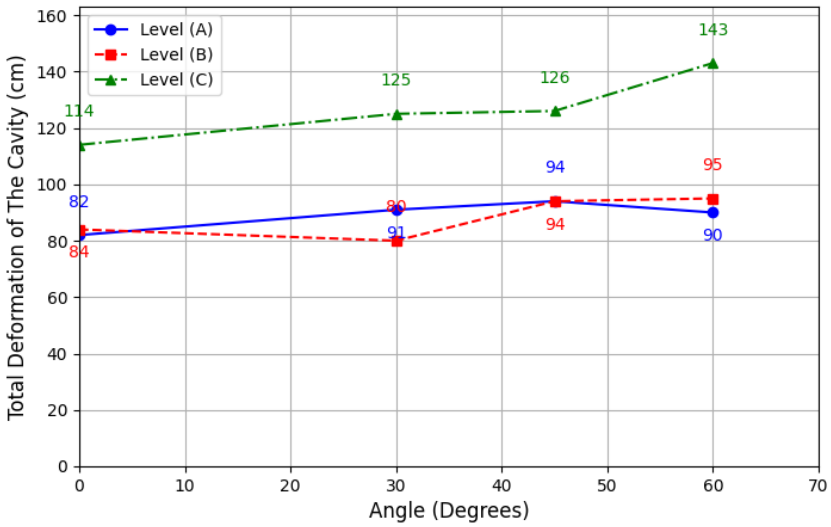

Fig. 11. Total displacement in different levels for different placement angles

The highest displacement was observed at level C in a placement angle of 60°, indicating a significant elevation of the cavern floor. This was due to interlayer passing near bottom of the cavern. As interlayer got closer to the bottom of the cavern, because of increasing stress resulted more deformation. The lowest displacement was observed at level B in placement angle of 30°. The total displacement at levels A and B is approximately similar.

C. Effect of interlayer number on total displacement

The geo21, geo22, and geo1 models were used to investigate the effect of interlayer numbers on displacement. In the geo21 model, two interlayers with a thickness of 10 meters passed through levels B and C, while in the geo22 model, three interlayers passed through levels A, B, and C. Fig. 12 shows the total displacement for model geo21, and Fig. 13 illustrates the effect of interlayer numbers on the total displacement.

Increasing the number of interlayers affected the total displacement. Two interlayers created more wall displacement than one interlayer. The reason is that increasing of interlayer numbers causes reduction of stiffness of media around the cavern.

D. Effect of interlayer numbers on equivalent strain

This study has shown that increasing the thickness of the interlayer has a more significant effect on total displacement than altering its placement angle.

Fig. 14. illustrated the effect of the interlayer level on the equivalent strain in the salt cavern after 15 years of operation. The distribution of equivalent strain indicated that areas with higher equivalent strain were frequently observed at the interlayer level.

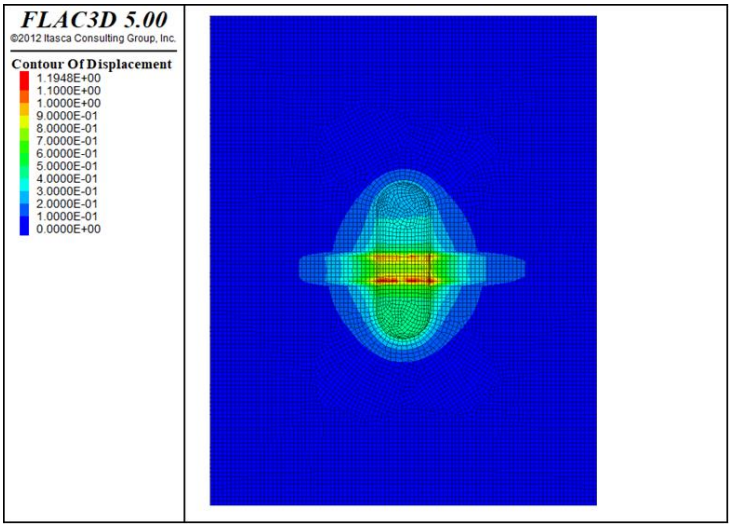

Fig. 12. Contour of total displacement for model geo21

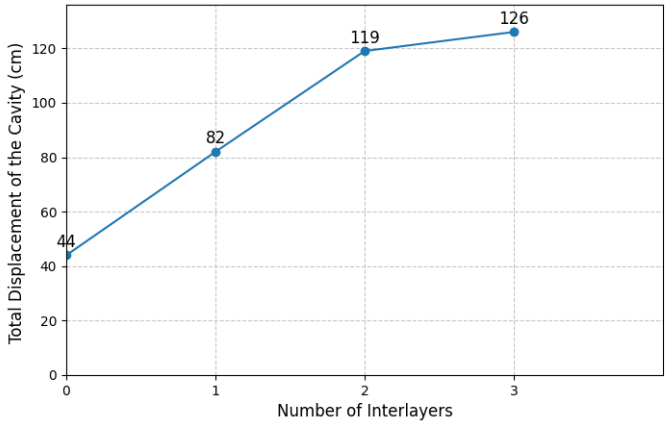

Fig. 13. Effect of interlayers numbers on total displacemen

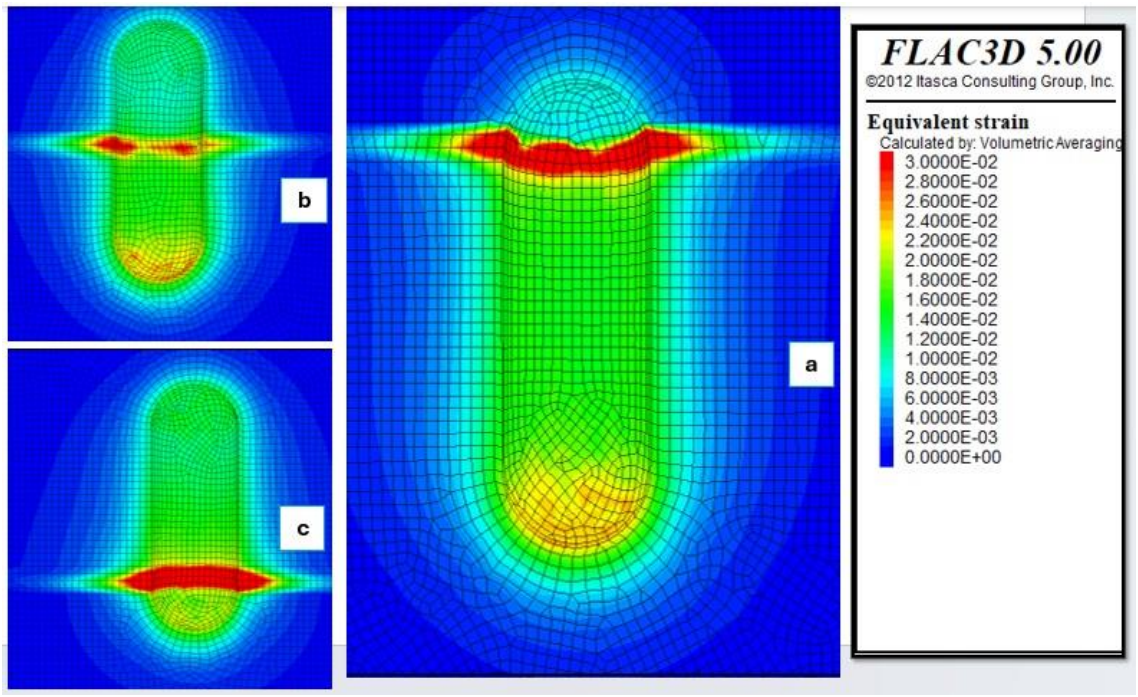

Fig. 14. Equivalent strain contour around the salt cavern: a) Interlayer at level A, b) Interlayer at level B, and c) Interlayer at level C

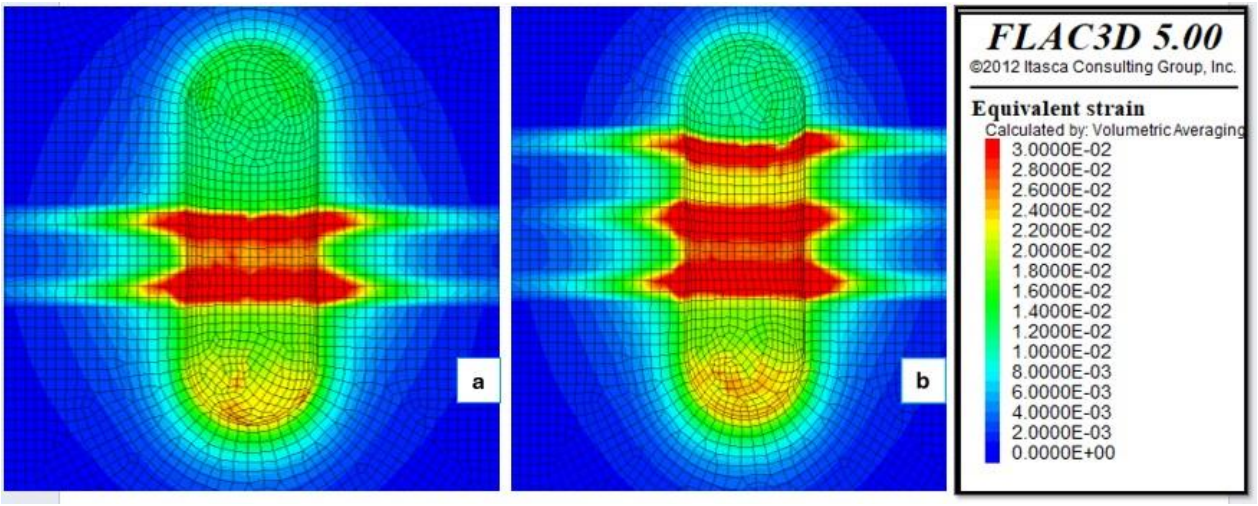

Fig. 15. Equivalent strain contour around the salt cavern: a) Two interlayers and b) Three interlayers

Fig. 14 showed red areas at the interlayers which indicated regions of high strain. At the bottom of the cavern (Level C), the strain was significantly higher compared to levels A and B. When the interlayer passed through the middle of the cavern (Level B), the high-strain area became smaller. Fig. 15 demonstrated how increasing the number of interlayers impacted the equivalent strain around the salt cavern.Increasing the number of interlayers effectively increased the areas with high equivalent strain which could reduce stability of cavern.

E. Effect of interlayers on dilatancy safety factor

For stability analysis, the dilatancy safety factor (Ratigan) was studied. During execution of the models, changes in the principal stress at the points (shown in Fig. 3) of salt cavern were recorded. Then, based on the dilatancy safety factor, changes in this factor were calculated at the points over operational time. The following sections present the graphs of the dilatancy safety factor changes during operational time (Fig. 16 and Fig. 17).

The dilatancy safety factor exhibited a cyclic pattern due to the injection and withdrawal of gas in the salt cavern during its operational time. Internal pressure fluctuations resulted in corresponding cyclic changes in the dilatancy safety factor. When the gas volume in the salt cavern reached its maximum, the highest dilatancy safety factor values were observed. Conversely, the minimum values were observed when gas was extracted, reducing the gas volume to its lowest point.

Fig. 17, higher values were excluded to better observation and studying the critical values of dilatancy safety factor. The critical value at point 1 for the geo22 model is 1.88. An analysis of the maximum principal stress showed that the geometric parameters of the interlayer such as thickness and placement angle did not affect the maximum value of the principal stress. The maximum principal stress was influenced mainly by overburden and variation of cavern internal pressure. Consequently, the dilatancy safety factor was not suitable criterion for evaluating the effect of the interlayer geometric parameters on the stability of salt cavern. Fig. 18. showed the second invariant contour of the invariant deviatoric stress J_2 after 15 years operational time of the geo22 model.

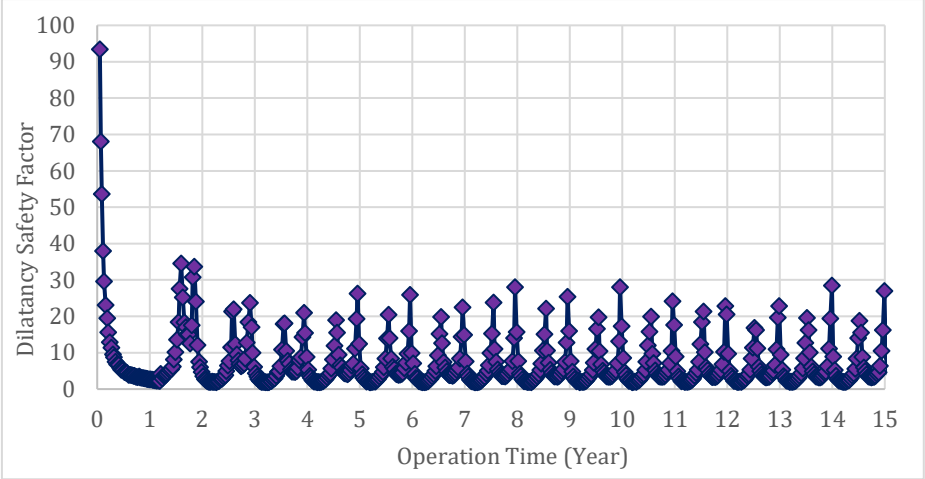

Fig. 16. Dilatancy safety factor for operational time of point 1(cavern roof) for the geo22 model

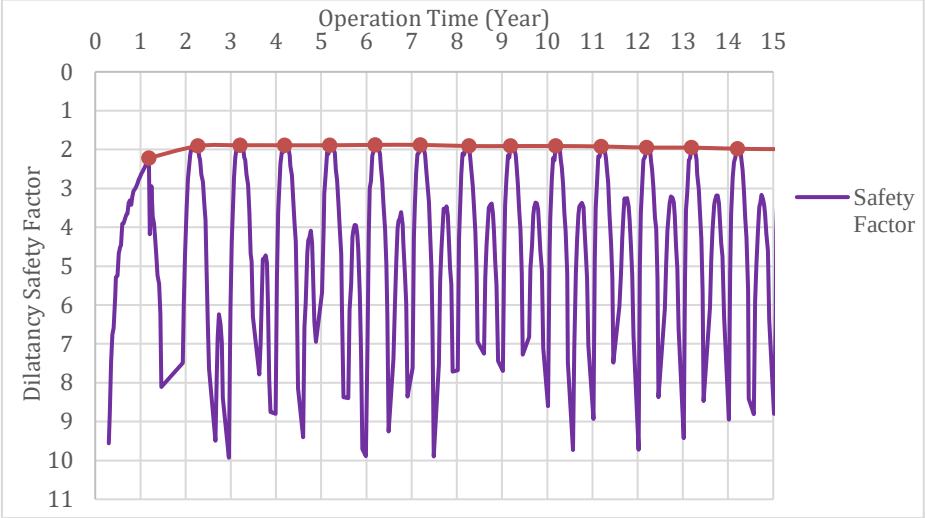

Fig. 17. Variations of the dilatancy safety factor vs. operational time at point 1 (cavern roof) for geo22 model and envelope on graph

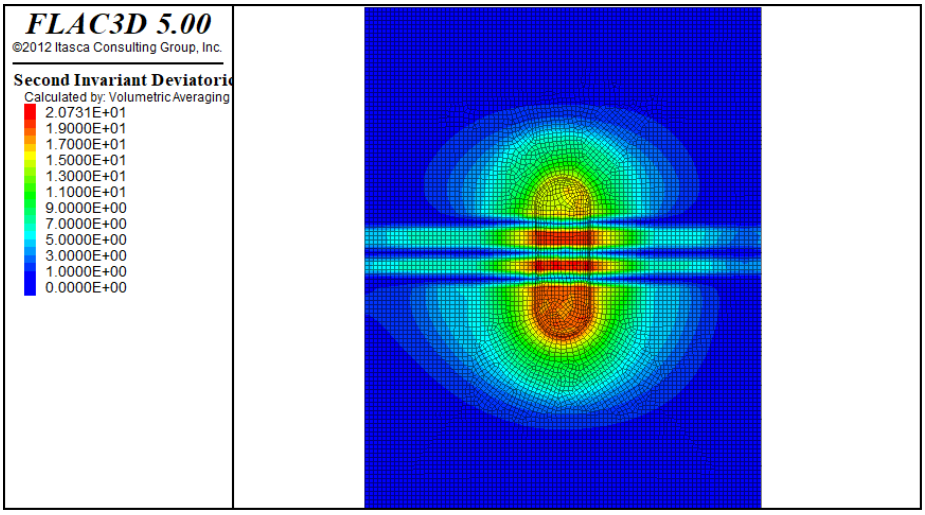

Fig. 18. Contour of second invariant deviatoric stress (J_2) after 15 years of operational time for model geo22

In the geo0 model, where there is no interlayer, the value of J_2 was 19.6 MPa. In subsequent models with an interlayer, a sharp reduction in deviatoric stresses was observed at the interlayer level, attributed to stress release due to the high displacement of the interlayers. The maximum deviatoric stresses occurred at the lower boundary between the rock salt and the interlayer. In Fig. 18, the maximum deviatoric stress increased to 20.7 MPa. Variations of stress and displacement were caused by increasing thickness and number of interlayers

which affecting the stability of salt cavern. Studying the deviatoric stress contour (J_2) showed that the presence of interlayers according to thickness, placement angle, number and level caused the redistribution of stresses and increased stresses at interface of the interlayer and rock salt. Additionally, an interlayer with lower stiffness led to higher deviatoric stresses.

VI. CONCLUSIONS

This study investigated the effects of interlayer thickness, placement angle, level, and number on the stability and deformation of salt caverns using FLAC3D software. The findings highlight the significant role of interlayer properties in influencing the long-term behavior of salt caverns, especially in terms of displacement, strain, and safety. The key conclusions from this investigation are as follows:

A. Effect of interlayer thickness

Increasing the thickness of the interlayer significantly raised the total displacement of the salt cavern. For instance, the displacement increased from 82 cm in the model with a 10 m thick horizontal interlayer (geo1) to 159 cm with a 20 m thick interlayer at a 30° placement angle. The presence of a weak interlayer amplified deformation, particularly near the interface between the salt rock and the interlayer. The displacement also exhibited a directional dependence, with larger displacements observed along the *X*, *Y*, and *Z* axes as interlayer thickness increased.

B. Effect of placement angle and level

The placement angle of the interlayer had a considerable impact on displacement, with the maximum deformation occurring at 60°. Displacement along the *Z*-axis increased significantly as the interlayer's angle of inclination increased, particularly near the cavern roof. The level of the interlayer also played a critical role in the distribution of displacements. Interlayers located near the floor (level C) caused greater deformation in the cavern floor and surrounding areas compared to interlayers positioned near the roof or middle.

C. Effect of interlayer number on total displacement

The number of interlayers directly influenced the total displacement, with multiple interlayers leading to larger deformations. The models with two and three interlayers (geo21 and geo22) showed higher displacements than the single interlayer model (geo1), as the increased number of interlayers reduced the stiffness of the surrounding media, making the cavern more susceptible to displacement.

D. Effect of interlayers on equivalent strain

Increasing the interlayer thickness and number resulted in higher equivalent strain, particularly at the interlayer levels. The strain distribution showed that areas near the interlayer, especially at the bottom of the cavern (level C), experienced significantly higher strain compared to the upper levels. Multiple interlayers amplified these strain areas, indicating a potential reduction in the cavern's stability over time.

E. Dilatancy safety factor

The dilatancy safety factor showed a cyclic behavior in response to gas injection and withdrawal during cavern operation. However, the results indicated that the dilatancy safety factor was not a reliable criterion for assessing the impact of interlayer geometric parameters on cavern stability. Variations in internal gas pressure and overburden had a more substantial effect on the safety factor than changes in the interlayer's thickness or angle. This suggests that the dilatancy safety factor is insufficient for evaluating the long-term stability of salt caverns with interlayers.

F. Effect of deviatoric stress on stability

The presence of interlayers caused a redistribution of deviatoric stresses, with maximum stresses observed at the interface between the salt rock and the interlayer. Increasing the interlayer thickness and number of interlayers led to a reduction in deviatoric stresses within the interlayer but an increase at the boundary, indicating that the interlayer could act as a zone of stress concentration. This behavior was especially pronounced, when interlayers with lower stiffness were present which contributed to higher deviatoric stresses and potential instability at the cavern boundaries.

Overall, the results suggest that the construction of salt caverns in salt layers with weak intermediate layers should be carefully evaluated. Increasing interlayer thickness, number, and proximity to the cavern floor enhances the risk of significant deformation and instability. The findings emphasize the importance of considering interlayer properties in the design and operation of salt caverns to ensure long-term stability and safety.

References

Asgari, A., Ramezanzadeh, A., Jalali, S. M., & Brouard, B. (2020). Stability analysis of salt cavern gas storage using 2D thermo-hydro-mechanical finite-element software. Journal of Mining and Environment, 11(1), 77-97.

Günther, R.-M., Salzer, K., Popp, T., & Lüdeling, C. (2015). Steady-state creep of rock salt: improved approaches for lab determination and modelling. Rock mechanics and rock engineering, 48, 2603-2613.

Langer, M., & Heusermann, S. (2001). Geomechanical stability and integrity of waste disposal mines in salt structures. Engineering geology, 61(2-3), 155-161.

Li, D., Liu, W., Jiang, D., Chen, J., Fan, J., & Qiao, W. (2021). Quantitative investigation on the stability of salt cavity gas storage with multiple interlayers above the cavity roof. Journal of Energy Storage, 44, 103298.

Li, M., Zhang, H., Xing, W., Hou, Z., & Were, P. (2015). Study of the relationship between surface subsidence and internal pressure in salt caverns. Environmental Earth Sciences, 73, 6899-6910.

Li, P., Li, Y., Shi, X., Zhao, A., Hao, S., Gong, X., Jiang, S., & Liu, Y. (2021). Stability analysis of U-shaped horizontal salt cavern for underground natural gas storage. Journal of Energy Storage, 38, 102541.

Liang, G.-C., Huang, X., Peng, X.-Y., Tian, Y., & Yu, Y.-h. (2016). Investigation on the cavity evolution of underground salt cavern gas storages. Journal of Natural Gas Science and Engineering, 33, 118-134.

Liu, W., Zhang, Z., Fan, J., Jiang, D., & Daemen, J. J. (2020). Research on the stability and treatments of natural gas storage caverns with different shapes in bedded salt rocks. Ieee Access, 8, 18995-19007.

Ma, H., Yang, C., Qi, Z., Li, Y., & Hao, R. (2012). Experimental and numerical analysis of salt cavern convergence in ultra-deep bedded formation. ARMA US Rock Mechanics/Geomechanics Symposium,

Mortazavi, A., & Nasab, H. (2017). Analysis of the behavior of large underground oil storage caverns in salt rock. International Journal for Numerical and Analytical Methods in Geomechanics, 41(4), 602-624.

Peng, J., Zhou, J., Liang, G., Peng, C., Hu, C., & Guo, D. (2023). Investigation on the long-term stability of multiple salt caverns underground gas storage with interlayers. Journal of Energy Resources Technology, 145(8), 081202.

Plaat, H. (2009). Underground gas storage: Why and how. Geological Society, London, Special Publications, 313(1), 25-37.

Shahmorad, Z., Salarirad, H., & Molladavoudi, H. (2016). A study on the effect of utilizing different constitutive models in the stability analysis of an underground gas storage within a salt structure. Journal of Natural Gas Science and Engineering, 33, 808-820.

Van Sambeek, L. L. (1986). Creep of rock salt under inhomogeneous stress conditions.

Wang, G., Guo, K., Christianson, M., & Konietzky, H. (2011). Deformation characteristics of rock salt with mudstone interbeds surrounding gas and oil storage cavern. International Journal of Rock Mechanics and Mining Sciences, 48(6), 871-877.

Wang, T., Ma, H., Shi, X., Yang, C., Zhang, N., Li, J., Ding, S., & Daemen, J. (2018). Salt cavern gas storage in an ultra-deep formation in Hubei, China. International Journal of Rock Mechanics and Mining Sciences, 102, 57-70.

Wang, T., Yang, C., Ma, H., Li, Y., Shi, X., Li, J., & Daemen, J. (2016). Safety evaluation of salt cavern gas storage close to an old cavern. International Journal of Rock Mechanics and Mining Sciences, 83, 95-106.

Wei, L., Yinping, L., Chunhe, Y., Deyi, J., Daemen, J., Jie, C., & Junfeng, K. (2016). A new method of surface subsidence prediction for natural gas storage cavern in bedded rock salts. Environmental Earth Sciences, 75, 1-17.

Xing, W., Zhao, J., Hou, Z., Were, P., Li, M., & Wang, G. (2015). Horizontal natural gas caverns in thin-bedded rock salt formations. Environmental Earth Sciences, 73, 6973-6985.

Yang, C., Wang, T., Li, J., Ma, H., Shi, X., & Daemen, J. (2016). Feasibility analysis of using closely spaced caverns in bedded rock salt for underground gas storage: a case study. Environmental Earth Sciences, 75, 1-15.

Yang, C., Wang, T., Li, Y., Yang, H., Li, J., Xu, B., Yang, Y., & Daemen, J. (2015). Feasibility analysis of using abandoned salt caverns for large-scale underground energy storage in China. Applied Energy, 137, 467-481.

Zhang, G., Wu, Y., Wang, L., Zhang, K., Daemen, J. J., & Liu, W. (2015). Time-dependent subsidence prediction model and influence factor analysis for underground gas storages in bedded salt formations. Engineering geology, 187, 156-169.

Zhang, N., Shi, X., Wang, T., Yang, C., Liu, W., Ma, H., & Daemen, J. (2017). Stability and availability evaluation of underground strategic petroleum reserve (SPR) caverns in bedded rock salt of Jintan, China. Energy, 134, 504-514.

Zhang, Q., Song, Z., Wang, J., Zhang, Y., & Wang, T. (2021). Creep properties and constitutive model of salt rock. Advances in Civil Engineering, 2021(1), 8867673.

Zhou, J., Peng, J., Huang, X., Chen, Y., Liang, G., & Li, Q. (2022). Research on long-term operation stability of salt rock underground gas storage with interlayers. Arabian Journal of Geosciences, 15(5), 389.